

NADPH Oxidase and Hydrogen Peroxide Mediate Insulin-induced Calcium Increase in Skeletal Muscle Cells*

Received for publication, June 3, 2008, and in revised form, October 27, 2008. Published, JBC Papers in Press, November 20, 2008, DOI 10.1074/jbc.M804249200

Alejandra Espinosa[‡], Alejandra García[§], Steffen Härtel^{¶1}, Cecilia Hidalgo^{§||2}, and Enrique Jaimovich^{§||2}

From the [‡]Escuela de Tecnología Médica, Facultad de Medicina, Universidad de Chile, Independencia 1027, Santiago 7, the [§]Centro de Estudios Moleculares de la Célula, Facultad de Medicina, Universidad de Chile, Santiago 7, the [¶]Programa de Anatomía y Biología del Desarrollo, Instituto de Ciencias Biomédicas (ICBM), Facultad de Medicina, Universidad de Chile, Santiago 7, and the ^{||}Programa de Biología Molecular y Celular, ICBM, Facultad de Medicina, Universidad de Chile, Santiago 7, Chile

Skeletal muscle is one of the main physiological targets of insulin, a hormone that triggers a complex signaling cascade and that enhances the production of reactive oxygen species (ROS) in different cell types. ROS, currently considered second messengers, produce redox modifications in proteins such as ion channels that induce changes in their functional properties. In myotubes, insulin also enhances calcium release from intracellular stores. In this work, we studied in myotubes whether insulin stimulated ROS production and investigated the mechanisms underlying the insulin-dependent calcium increase: in particular, whether the late phase of the Ca²⁺ increase induced by insulin required ROS. We found that insulin stimulated ROS production, as detected with the probe 2', 7'-dichlorofluorescein diacetate (CM-H₂DCFDA). We used the translocation of p47^{phox} from the cytoplasm to the plasma membrane as a marker of the activation of NADPH oxidase. Insulin-stimulated ROS generation was suppressed by the NADPH oxidase inhibitor apocynin and by small interfering RNA against p47^{phox}, a regulatory NADPH oxidase subunit. Additionally, both protein kinase C and phosphatidylinositol 3-kinase are presumably involved in insulin-induced ROS generation because bisindolylmaleimide, a nonspecific protein kinase C inhibitor, and LY290042, an inhibitor of phosphatidylinositol 3-kinase, inhibited this increase. Bisindolylmaleimide, LY290042, apocynin, small interfering RNA against p47^{phox}, and two drugs that interfere with inositol 1,4,5-trisphosphate-mediated Ca²⁺ release, xestospongine C and U73122, inhibited the intracellular Ca²⁺ increase produced by insulin. These combined results strongly suggest that insulin induces ROS generation through NADPH activation and that this ROS increase is required for the intracellular Ca²⁺ rise mediated by inositol 1,4,5-trisphosphate receptors.

A transient intracellular Ca²⁺ increase is a key component of the excitation-coupling mechanism in skeletal muscle cells. Intracellular Ca²⁺ can also increase in response to stimuli other

than membrane potential depolarization, including hormones such as insulin. We have previously reported that in myotubes, the addition of insulin produces a fast intracellular Ca²⁺ concentration transient, which requires external Ca²⁺ and is inhibited by the L-type Ca²⁺ channel blocker nifedipine and by ryanodine (1). Other reports show that the Ca²⁺ increase evoked by insulin in skeletal muscle fibers depends on Ca²⁺ influx and is related to Glut-4 translocation (2). As steep changes in insulin concentration are unlikely to occur physiologically, we decided to explore changes in intracellular Ca²⁺ after longer exposure to insulin. We further investigated whether ROS³ play a role in this process. It is known that ROS modulate the activity of Ca²⁺ release channels (3), and in particular, the activity of skeletal muscle ryanodine receptors is regulated by NADPH oxidase-dependent redox modifications (4). On the other hand, in target tissues, insulin is known to generate ROS, which participate in signaling processes triggered by the hormone (5).

There are many intracellular sources of ROS in mammalian cells, such as mitochondria, xanthine oxidase, and NADPH oxidase (6, 7). We have reported the presence of NADPH oxidase subunits in myotubes (1) and in adult skeletal muscle transverse tubules (4). Recently, the NADPH oxidase has been involved in modifications of tyrosine phosphates that shut down signals evoked by insulin in adipocytes (8). The phagocytic NADPH oxidase is composed of five subunits: two catalytic subunits located in the plasma membrane (p22^{phox} and gp91^{phox}) and three cytoplasmic subunits (p40^{phox}, p47^{phox}, and p67^{phox}), plus the small GTP-binding protein rac-1. Upon activation, these subunits translocate to the plasma membrane to form the active enzyme (9). The regulatory p47^{phox} subunit has an autoinhibitory domain; phosphorylation of p47^{phox} in serine residues causes its translocation to the plasma membrane to form the active enzymatic complex. Activation of p47^{phox} depends on several serine/threonine and tyrosine kinases such as protein kinase C (PKC) (10, 11), c-Src (12), and phosphatidylinositol 3-kinase (PI3K) (13).

* This work was supported by Fondo Nacional de Investigación en Areas Prioritarias (FONDAP) Grant 15010006. The costs of publication of this article were defrayed in part by the payment of page charges. This article must therefore be hereby marked "advertisement" in accordance with 18 U.S.C. Section 1734 solely to indicate this fact.

¹ Supported by Fondecyt Grants 1060890, 1071001, and PBCT ACT47.

² To whom correspondence should be addressed: ICBM, Facultad de Medicina, Universidad de Chile, Casilla 70005, Santiago 7, Chile. Tel.: 56-2-978-6510; Fax: 56-2-777-6916; E-mail: ejaimovi@med.uchile.cl.

³ The abbreviations used are: ROS, reactive oxygen species; PKC, protein kinase C; PKB, protein kinase B; PI3K, phosphatidylinositol 3-kinase; DAG, diacylglycerol; IP₃, inositol 1,4,5-trisphosphate; IP₃R, IP₃ receptor; fluo-3AM, fluo-3 acetoxymethyl ester; CM-H₂DCFDA, 7'-dichlorofluorescein diacetate; DsRed, red fluorescent protein; BTK, Bruton's tyrosine kinase; PH, pleckstrin homology; GFP, green fluorescent protein; ROI, region of interest; DMSO, dimethyl sulfoxide; siRNA, small interfering RNA; BIM, bisindolylmaleimide; IRS-1, insulin receptor substrate-1.

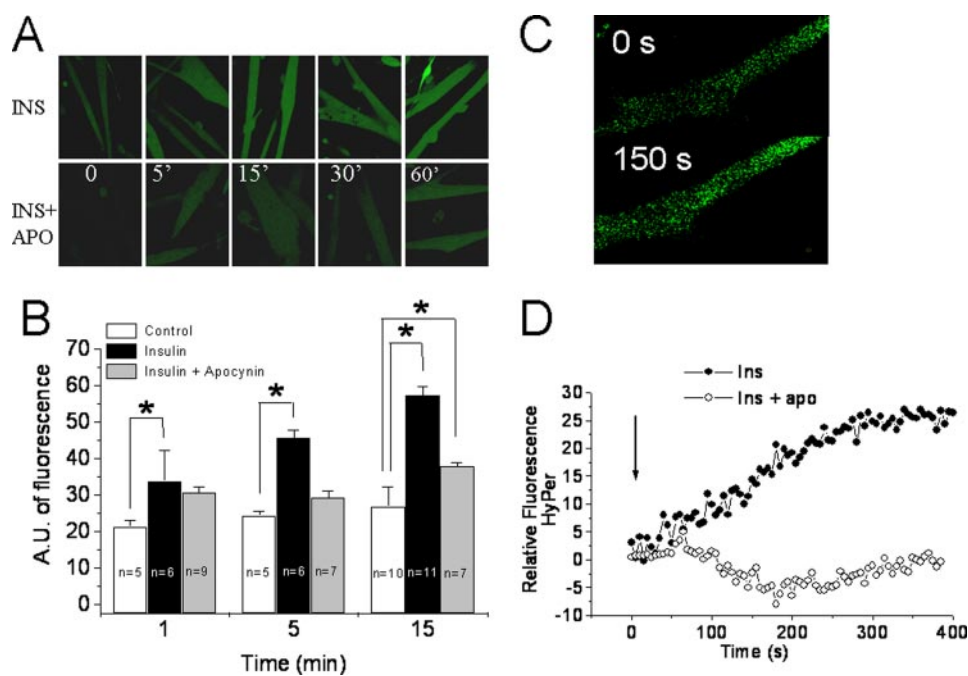


FIGURE 1. Insulin-induced H₂O₂ generation. *A*, sequence of images acquired in basal conditions and after insulin (INS) stimulation at the times indicated (upper sequence). The effect of apocynin (APO) on the same conditions is shown in the lower panel. *B*, the graph represents mean fluorescence values of CM-H₂DCFDA in arbitrary units (A.U.) at indicated times after 50 nM insulin addition, in the absence or presence of apocynin. Myotubes were loaded with CM-H₂DCFDA for 15 min, and fluorescence was measured in a confocal microscope using 0.5% of laser potency (indicated *n* values correspond to three different cultures, *p* < 0.05 (*)). To detect H₂O₂, we used a molecular probe based in HyPer protein. *C*, fluorescence images of myotubes transfected with the HyPer plasmid, before and after 50 nM insulin stimulation. *D*, representative time sequences of fluorescence in myotubes transfected with HyPer, in the absence or presence of apocynin. The arrow shows insulin addition. Images were acquired every 5 s.

By inducing phosphorylation of its receptor on tyrosine residues, insulin initiates a well described signal transduction cascade (14), which involves PI3K activation. Insulin can also activate phospholipase C and generate IP₃ and diacylglycerol (DAG). These second messengers can induce Ca²⁺ release and PKC activation, respectively. The main goal of this work was to investigate the possible correlation between the increase in Ca²⁺ and ROS induced by insulin. We found that both PI3K and PKC are needed to activate NADPH oxidase to produce ROS and that ROS are involved in the delayed Ca²⁺ increase induced by insulin, which involves IP₃ receptor (IP₃R) activation by ROS.

EXPERIMENTAL PROCEDURES

Reagents—Insulin, fluo-3 acetoxymethyl ester (fluo-3AM), Alexa Fluor 488 and Alexa Fluor 633, and chloromethyl-2,7-dichlorodihydrofluorescein diacetate (CM-H₂DCFDA) were purchased from Invitrogen. Bordetella pertussis toxin was obtained from Calbiochem. Xestospongin C was a gift from Dr. Jordi Molgò (Centre National de la Recherche Scientifique, Gif-sur-Yvette, France). Antibodies against insulin receptor, p47^{phox} and gp91^{phox}, were obtained from Santa Cruz Biotechnology (Santa Cruz, CA). Horseradish peroxidase-linked anti-rabbit and anti-mouse IgG were purchased from Pierce. A plasmid encoding DsRed (Clontech) was used as a transfection marker.

The plasmids used encode the fusion protein between the pleckstrin homology (PH) domain of Bruton's tyrosine kinase

(BTK) and the enhanced green fluorescent protein (GFP) ((PH)BTK-GFP) or the (PHmut)BTK-GFP (punctual mutation R28C of the PH domain). Both plasmids were kindly provided by Dr. Tamas Balla (National Institutes of Health, Bethesda, MD). A plasmid that encodes for HyPer protein was acquired from Evrogen Joint Stock Company, Moscow, Russia.

Cell Culture—Primary cultured cells were obtained from rat neonatal hind limbs. The muscle tissue was mechanically dispersed and then incubated under mild agitation with 10% (w/v) collagenase for 15 min at 37 °C. The suspension was filtered through a Nutex (Sartorius, Göttingen, Germany) membrane and spun down at low speed, preplating was used to partially eliminate fibroblasts, and finally, cells were plated onto dishes (60 mm) with coverslips at a density of 0.6 × 10⁶/dish. The culture medium used was Dulbecco's modified Eagle's medium/F-12, 10% bovine serum, 2.5% fetal calf serum, 100 mg/liter penicillin, 50 mg/liter streptomycin,

and 2.5 mg/liter amphotericin B. To eliminate remaining fibroblasts, on the third day of culture, 10 μM cytosine arabinoside was added for 24 h. The medium was then replaced with serum-free medium. 6–8-day-old cultures were used.

Ca²⁺ Measurement—Cytoplasmic Ca²⁺ images were obtained using inverted confocal microscopy (Carl Zeiss Pascal 5 LSM) from single, non-spontaneously contracting myotubes preloaded with fluo-3AM. Myotubes were washed with Krebs buffer (10 mM Hepes-Na, pH 7.4, 145 mM NaCl, 5 mM KCl, 2.6 mM CaCl₂, 1 mM MgCl₂, 5.6 mM glucose,) and loaded with 5.4 μM fluo-3AM (added from a stock solution in 20% pluronic acid-DMSO) for 30 min at room temperature. Cell-containing coverslips were mounted in a 1-ml capacity plastic chamber and placed in the microscope for fluorescence measurements (band pass 505–530 nm) after excitation with a 488 nm argon laser.

Determination of ROS Production—ROS generation was determined in skeletal muscle cells using CM-H₂DCFDA. Myotubes were cultured on glass coverslips and incubated with 5 μM CM-H₂DCFDA for 15 min at 37 °C. Cells on coverslips were washed with PBS and placed at the bottom of an incubation chamber, which was transferred to the confocal microscope. CM-H₂DCFDA fluorescence was detected using excitation/emission wavelengths λ_{exc}/λ_{em} = 488/505–530 nm. In all measurements a control of the effect of laser excitation alone was performed. Noise in the images was removed by the Image J software (National Institutes of Health).

Immunofluorescence—Cells were placed on coverslips and fixed with methanol at –20 °C for 15 min. The blockade was

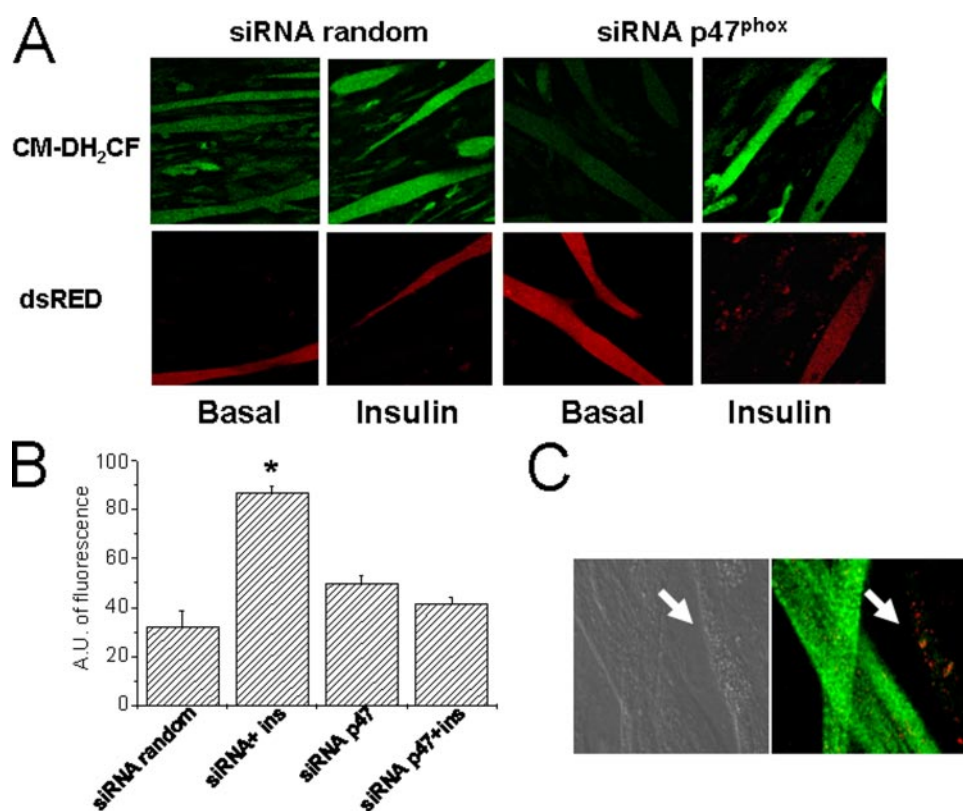


FIGURE 2. **p47^{phox} is involved in ROS generation.** *A*, a representative panel of images showing CM-H₂DCFDA fluorescence increase in myotubes co-transfected with siRNA against p47^{phox} (siRNA p47^{phox}) or a random control, and DsRed. Myotubes were loaded with CM-H₂DCFDA and then stimulated with insulin. The lower panel shows DsRed fluorescence as a transfection control. In the stimulated condition, myotubes were incubated with 50 nM insulin for 15 min. *B*, mean values of fluorescence in arbitrary units (A.U.) from the experiments described in *A*. The graph represents mean of values from 4 to 6 cells from 3 different experiments, $p < 0.05$ (*). *Ins*, insulin. *C*, immunofluorescence against p47^{phox} in myotubes co-transfected with DsRed and siRNA against p47^{phox}. Myotubes showing red fluorescence (arrow) do not react with anti-p47^{phox} antibody. The left panel shows the transmitted light image.

performed in 1% bovine serum albumin for 60 min, and the primary antibodies were incubated overnight at 4 °C. Cells were washed and incubated with secondary antibody during 2 h at room temperature. Coverslips were mounted in VECTASHIELD (Vector Laboratories, Inc.) for confocal microscopy, and representative images were acquired. Negative controls used only secondary antibodies.

Image Capture and Quantification of Fluorescence—Confocal image stacks were captured with a Zeiss LSM-5, Pascal 5 Axiovert 200 microscope, using LSM 5.3.2 image capture, analysis software, and a Plan-Apochromat ×63/1.4 oil differential interference contrast objective. Two-channel fluorescent image stacks (intensity $I(x,y,z)$, voxel size $\Delta x/\Delta y/\Delta z = 50/50/300$ nm) were recorded in the multitrack mode. Channel-1 (Alexa Fluor 488) was used with excitation/emission wavelengths $\lambda_{exc}/\lambda_{em} = 488/505\text{--}530$ nm, and channel-2 (Alexa Fluor 633) was used with $\lambda_{exc}/\lambda_{em} = 635/>650$ nm. We made sure that $I(x,y,z)$ did not saturate and that the image background was slightly above zero by carefully adjusting the laser power, the detector gain, and the detector offset.

Image stacks were deconvoluted with Huygens Scripting (Scientific Volume Imaging, Hilversum, Netherlands). All following image processing routines were developed in our laboratory on the basis of IDL (Interactive Data Language,

ITT, Boulder, CO). To determine p47^{phox} in the plasma membrane and the cytoplasm of myotubes, segmentations were performed to define different regions of interest (ROIs). First, the cross-section of myotubes was segmented by an intensity threshold in the green fluorescence channel (see Fig. 3D, center). Remaining holes inside the cells and artifacts outside the cells were filled or removed by morphological filters. Second, we used a border detection filter to identify the plasma membrane with a constant thickness of 400 nm (see Fig. 3D, right). The nuclear region was defined manually using the bright field image and excluded from the segmented cells. The fluorescence intensities of the cytoplasm and the plasma membrane were determined in the ROIs and divided by the respective surfaces ($I/\mu\text{m}^2$). For all experiments, the protocols remained constant, and the quality of the segmentation was controlled interactively by overlaying the original fluorescence images with the segmented ROIs.

Co-localization Analysis—A reliable segmentation of cellular structures containing p47^{phox} or α -actinin could not be obtained by a simple threshold value in fluorescence intensity because background intensities vary within the cell thickness across the image. We solved this problem by applying gradient filters and selecting threshold values in the gradient histograms, which resulted in a homogeneous definition of p47^{phox} or α -actinin signals (see Fig. 3A).

For the quantification of co-localization between p47^{phox} and α -actinin (Fig. 3A, left, ROI1/green regions and ROI2/red regions), we calculated the Manders co-localization coefficients M_1 and M_2 (15). M_1 and M_2 sum up the contribution of the respective fluorescence intensities in the co-localizing region $I_{Ch1/2}(ROI1 \cap ROI2)$, and we divided the number by the sum of the fluorescence intensities inside of the segmented regions $I_{Ch1}(ROI1)$ or $I_{Ch2}(ROI2)$. M_1 and M_2 can be interpreted directly as the amount of co-localizing p47^{phox}/ α -actinin labeled structures (Fig. 3A, lower, yellow regions) with respect to the total amount of segmented p47^{phox}/ α -actinin signals (Fig. 3A, lower left panel, yellow region plus green/red region). To reveal the significance of the co-localization coefficients, we implemented a defined displacement algorithm (16). Defined displacement algorithm shifts one fluorescent channel with respect to the second channel in a radial manner and calculates M_1 and M_2 successively for each displacement. When the radial displacement is larger

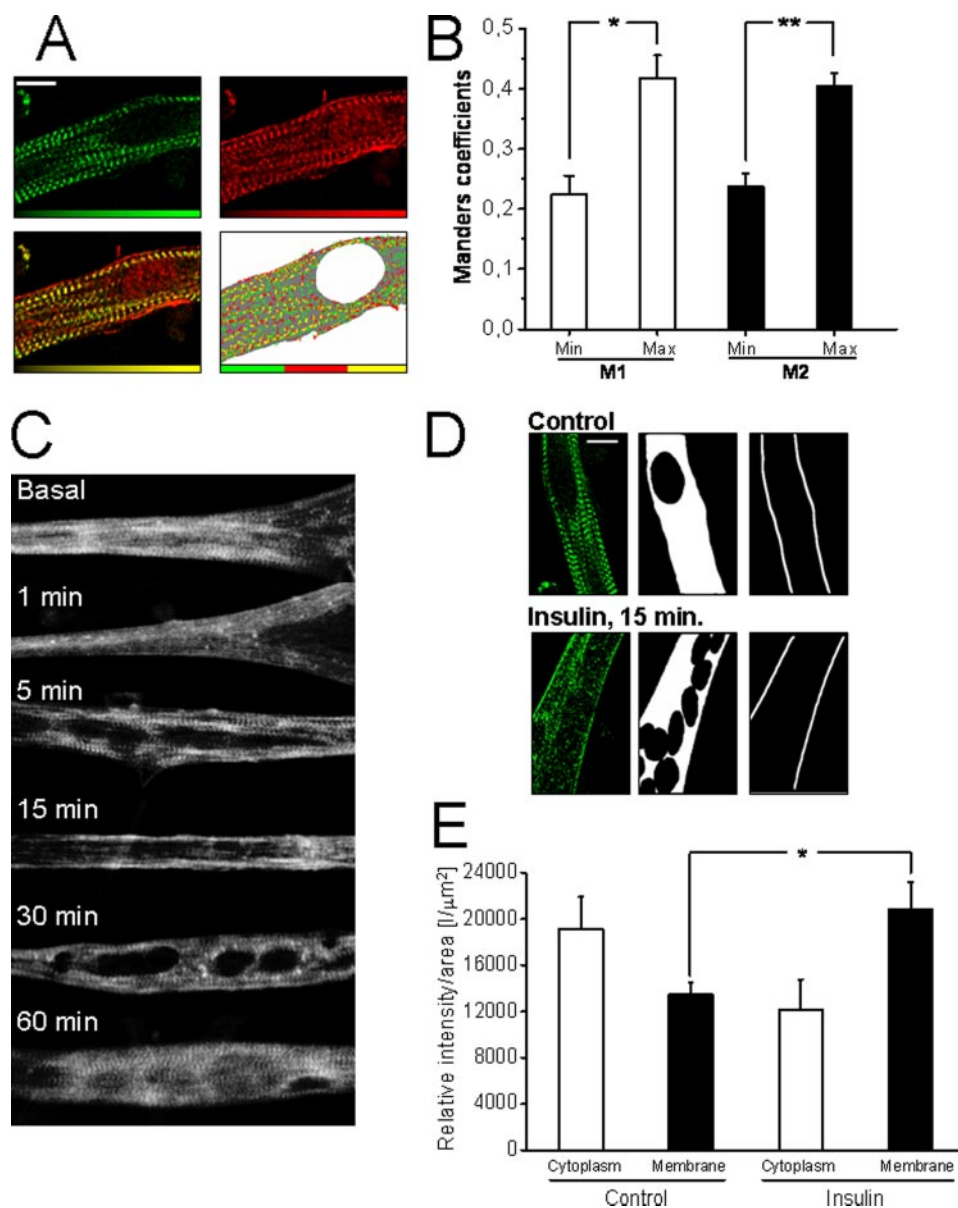


FIGURE 3. p47^{phox} co-localizes with Z-bands in myotubes and translocates to the plasma membrane 15 min after insulin stimulus. *A*, representative immunofluorescence images show the distribution of p47^{phox} and α -actinin (green and red channels) and the merged image (lower left panel). Confocal images were deconvoluted and segmented according to the methodology described under "Results." Manders co-localization coefficients were calculated based on the segmentations of the ROIs (green, p47^{phox}; red, α -actinin; yellow, co-localization; gray, myotubes without nucleus, lower right panel). The scale bar represents 10 μm . *B*, Manders coefficients M_1 and M_2 show significant co-localization for both proteins. M_1 and M_2 maxima (Max) correspond to the mean Manders coefficients calculated at the initial image position. M_1 and M_2 minima (Min) are the mean values of the respective coefficients calculated for displacements that simulate random scenarios (*, $p < 0.001$, ** $p < 0.005$, $n = 3$, mean \pm S.E.). *C*, time sequence of immunofluorescence of p47^{phox} translocation in different representative myotubes fixed after stimulation with 50 nM insulin. *D*, representative immunofluorescence images (left) show the distribution of p47^{phox} in control and stimulated myotubes (upper and lower panels). Fluorescence intensities were determined inside the ROIs depicted in the center (cytoplasm) and right panels (region near plasma membrane) for both conditions. Fluorescence intensity values inside the ROIs were divided by the respective areas (total cross-section without nuclei and membrane). The scale bar represents 10 μm . *E*, fluorescence intensities of cytoplasm and cell membrane normalized by the respective areas. The mean values show a redistribution of p47^{phox} from the cytoplasm to the plasma membrane, 15 min after insulin stimulation. Although fluorescence inside the entire cross-section does not show significant changes (data not shown), p47^{phox} increases significantly in the region near the plasma membrane (*, $p < 0.008$, $n = 3$ independent experiments, mean \pm S.E.).

than the size of the segmented ROIs, the calculated Manders coefficients quantify random scenarios of fluorescent structures inside the cellular borders, which were used to calculate the M_1/M_2 minima values in Fig. 3B.

duced a small decrease of the initial endogenous levels of H_2O_2 (Fig. 1D).

Role of the p47^{phox} Subunit in ROS Generated by Insulin—The results obtained with apocynin strongly suggest that a

Data Analysis—All experiments were performed in at least three different cultures, and at least three cells per culture were measured in each case. Results are expressed as the mean \pm S.E. Significance was evaluated using Student's t test for paired data and one-way analysis of variance followed by Dunnett's post hoc test for multiple column comparison to control column; $p < 0.05$ was considered significant.

RESULTS

Insulin Induced ROS Generation through NADPH Oxidase Stimulation—Cultured myotubes preincubated with CM- H_2DCFDA were stimulated with insulin to investigate insulin-induced ROS generation. Fig. 1A shows a representative experiment where images were acquired at different times after the addition of 50 nM insulin. This concentration was chosen because of its clear-cut effects on calcium transient generation (see below). The time dependence of the mean fluorescence increase mediated by the hormone is presented in Fig. 1B. A significant increase in intracellular ROS was evident 5 min after insulin stimulation. Cells incubated with apocynin, a specific inhibitor of p47^{phox}-dependent NADPH oxidase ($\text{EC}_{50} = 10 \mu\text{M}$ (7)) displayed significantly reduced ROS production, and this effect was evident 5 min after insulin addition (Fig. 1B). To ascertain whether H_2O_2 is one of the ROS involved in this response, we used the HyPer protein, which is a genetically encoded fluorescent sensor for the specific detection of intracellular H_2O_2 (17). We measured the increase of HyPer fluorescence in myotubes after insulin stimulation. The increase in HyPer fluorescence was homogeneous in the cytoplasm of the myotube (Fig. 1C) and increased steadily in time, reaching a plateau of about 25-fold increase at 300 s; apocynin prevented this increase and even pro-

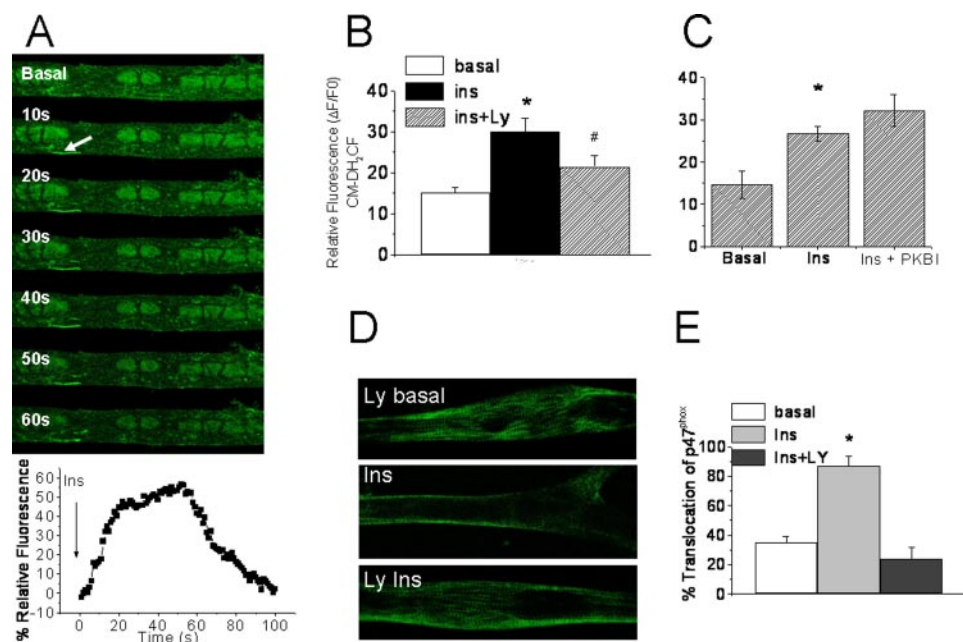


FIGURE 4. **The role of PI3K in ROS generation by insulin.** *A*, upper panel, time sequence of fluorescent images of a live myotube transfected with a fusion protein (including the PH domain of BTK and enhanced GFP), acquired by confocal microscopy every 10 s; the arrow indicates the presence of a fluorescent structure near the plasma membrane after insulin stimulation. Lower panel, a representative graph for fluorescence time course quantification near the membrane (upper panel, arrow). A.U., arbitrary units. *B*, mean fluorescence in myotubes loaded with CM-H₂DCFDA. Cells were preincubated with LY290042 (50 μM, Ly) for 30 min and were then stimulated with insulin. Fluorescence was measured 15 min after insulin stimulation ($n = 5-9$). *C*, myotubes were incubated with an inhibitor of PKB (PKBI), and then fluorescence was measured 15 min after insulin stimulation ($n = 8-10$). *D*, myotubes, control and incubated with LY290042, were stimulated with insulin (Ins) and then fixed with methanol for 15 min to label with specific antibody against p47^{phox} (representative images, $n = 5$). *E*, the relative number of myotubes in which p47^{phox} translocated from cytoplasm to membrane. Values are expressed as the percentage of cells in which translocation was evident ($n = 15$ from three independent cultures, $p < 0.05$ (*)).

p47^{phox}-dependent NADPH oxidase is involved in ROS generation. To test this hypothesis, we measured insulin-dependent CM-H₂DCFDA fluorescence in cells transfected with siRNA against p47^{phox}, using siRNA with a random sequence as control (Fig. 2A). To identify the transfected cells, they were co-transfected with a plasmid encoding DsRed protein. Red-labeled cells, transfected with the random sequence, responded with a fluorescence increase 10 min after insulin stimulation (Fig. 2A). In contrast, red-labeled cells transfected with siRNA against p47^{phox} did not respond to insulin, and the fluorescence signal was similar to that of cells expressing random siRNA in the basal state (Fig. 2, A and B). To evaluate whether p47^{phox} expression was decreased in myotubes transfected with siRNA, we performed an immunofluorescence study against the p47^{phox} subunit. The p47^{phox} subunit was not detected in cells transfected with siRNA p47^{phox} (Fig. 2C).

To study the insulin-dependent activation of NADPH oxidase, we determined by immunofluorescence the translocation of p47^{phox}. In basal conditions, p47^{phox} showed a particular distribution in myotubes; the label was present in striations and displayed a significant co-localization with α -actinin, a Z line marker protein (Fig. 3, A and B). In the first minute after insulin addition, some p47^{phox} label already appeared near the membrane (Fig. 3C, arrow). 15 min after stimulation, most of the label appeared in the periphery of myotubes, probably representing the location of the enzyme near the plasma membrane. At 60 min, the distribution of the fluorescence signal showed a

pattern similar to the basal condition prior to insulin addition (Fig. 3C). We measured fluorescence intensity in regions of the cytoplasm and near the plasma membrane (Fig. 3D). We defined the region near the plasma membrane with a constant diameter of 400 nm and the region inside the cytoplasm excluding cell nuclei (Fig. 3D, right and center). In the region near the plasma membrane, a significant fluorescence increase was detected after insulin stimulation (Fig. 3E). This membrane location was seen only in stimulated sections, never in basal conditions (Fig. 3C shows different times). Cytoplasmic fluorescence decreases upon stimulation (Fig. 3E) concomitant to the increase in near membrane fluorescence; as both myotubes (basal and stimulated) were measured in identical conditions, these observed differences suggest p47^{phox} translocation to the membrane region.

Role of PI3K in ROS Generation—PI3K activation is a key event in insulin-dependent signal transduction, so we studied whether ROS generation depends on PI3K activity.

Using a plasmid that encodes a fusion protein between the PH domain of BTK and the enhanced GFP ((PH)-BTK-GFP), we monitored the activation of PI3K as changes in probe fluorescence, considering that when PI3K is activated, it can recruit proteins with the PH domain to membranes. Cells transfected with (PH)-BTK-GFP showed basal fluorescence in nucleus and cytoplasm; 10 s after insulin stimulation, a distinct fluorescence increase appeared near the plasma membrane and in regions that may correspond to transverse tubules. This particular fluorescence increase disappeared after 90 s (Fig. 4A). These results indicate that activation of PI3K is an early event of the signal transduction cascade triggered by insulin that occurs prior to ROS generation. We next measured ROS generation induced by 50 nM insulin 15 min after stimulation in controls or in cells preincubated with different drugs. ROS production was completely prevented by genistein, an inhibitor of insulin receptor (Fig. 4B). LY290042, an inhibitor of the PI3K pathway, also produced a complete inhibition of fluorescence increase with respect to the control stimulated condition (Fig. 4B), suggesting that PI3K is a key player in ROS generation triggered by insulin. Previous reports suggest that PKB can phosphorylate p47^{phox}. To probe the role of PKB in ROS generation, we used a PKB inhibitor, PKBI (Fig. 4C, PKBI). We measured ROS generation 30 min after insulin stimulation and found similar values for ROS production both in the presence of inhibitor and in control conditions (Fig. 4C). Accordingly, we can conclude that insulin-stimulated ROS generation is dependent on PI3K but

not on PKB. To evaluate the participation of PI3K in the activation of NADPH oxidase, we studied the insulin-dependent translocation of p47^{phox} to the plasma membrane in the presence of LY290042. As shown above, p47^{phox} is present in the cytoplasm in basal conditions; after 10 min of insulin stimulation in the presence of LY290042, most of the label still remained in striations (Fig. 4C). There was some translocation in the presence of the inhibitor but clearly much less than in the control conditions illustrated in Fig. 3C.

Role of PKC in ROS Generation—To study the possible role of PKC in insulin-dependent ROS generation, we preincubated myotubes with BIM, a general inhibitor of PKC. Incubation with BIM inhibited insulin-induced ROS generation (Fig. 5A). In addition, 0.5 μM BIM inhibited the increase in HyPer fluorescence induced by insulin (Fig. 5C) and also prevented the translocation of p47^{phox} to the plasma membrane induced by insulin (Fig. 5B).

Insulin Increased the Intracellular Ca²⁺ Concentration in Cultured Myotubes—We had some evidence for delayed Ca²⁺ oscillations occurring after the fast Ca²⁺ transient induced by insulin in myotubes (1); these oscillations were seen at insulin concentrations as low as 1–10 nM but were consistently larger (80-fold increase in fluo-3 fluorescence) at 50 nM insulin. Accordingly, in this report, we performed a detailed study of these delayed Ca²⁺ signals in cultured myotubes using the fluorescence probe fluo-3AM. The insulin-dependent Ca²⁺ signals studied in this work are independent of the fast Ca²⁺ transients that require extracellular Ca²⁺ and functional ryanodine receptors (1). Thus, in conditions in which the fast transient is absent (*i.e.* in the absence of external Ca²⁺), the delayed signal remained unchanged, whereas inhibitors of the slow Ca²⁺ signal (see below) did not affect the fast Ca²⁺ signal (for example, Fig. 6C). We investigated the possible role of NADPH oxidase-generated ROS on the slower Ca²⁺ signals produced by insulin. To that aim, we measured the effect of both diphenyliodonium (Fig. 6A, DPI) and apocynin on insulin-evoked signals. Preincubation of myotubes with both inhibitors abolished the insulin-dependent intracellular Ca²⁺ increases (Fig. 6A). On the same line, we studied the role of NADPH oxidase using siRNA against p47^{phox}. Fig. 6B shows a representative response of transfected myotubes in which the Ca²⁺ increase produced by insulin was reduced significantly in myotubes transfected with siRNA against p47^{phox}. In addition, the PKC inhibitor BIM decreased significantly the insulin-dependent Ca²⁺ increase, whereas the PI3K inhibitors wortmannin and LY290042 completely prevented this response (Fig. 6C). To test the involvement of IP₃ receptors on Ca²⁺ signals, we preincubated the myotubes with two inhibitors of the IP₃ pathway, U73122 and xestospongin C; the insulin-stimulated Ca²⁺ increase was abolished in both conditions (Fig. 6D).

DISCUSSION

In this work, we provide evidence favoring a role for insulin in ROS generation due to NADPH oxidase activation in skeletal muscle cells. We show, in addition, that enhanced ROS generation forms part of the signaling mechanisms whereby insulin increases intracellular Ca²⁺ concentration. The fast increase of intracellular ROS produced by insulin was detected using both

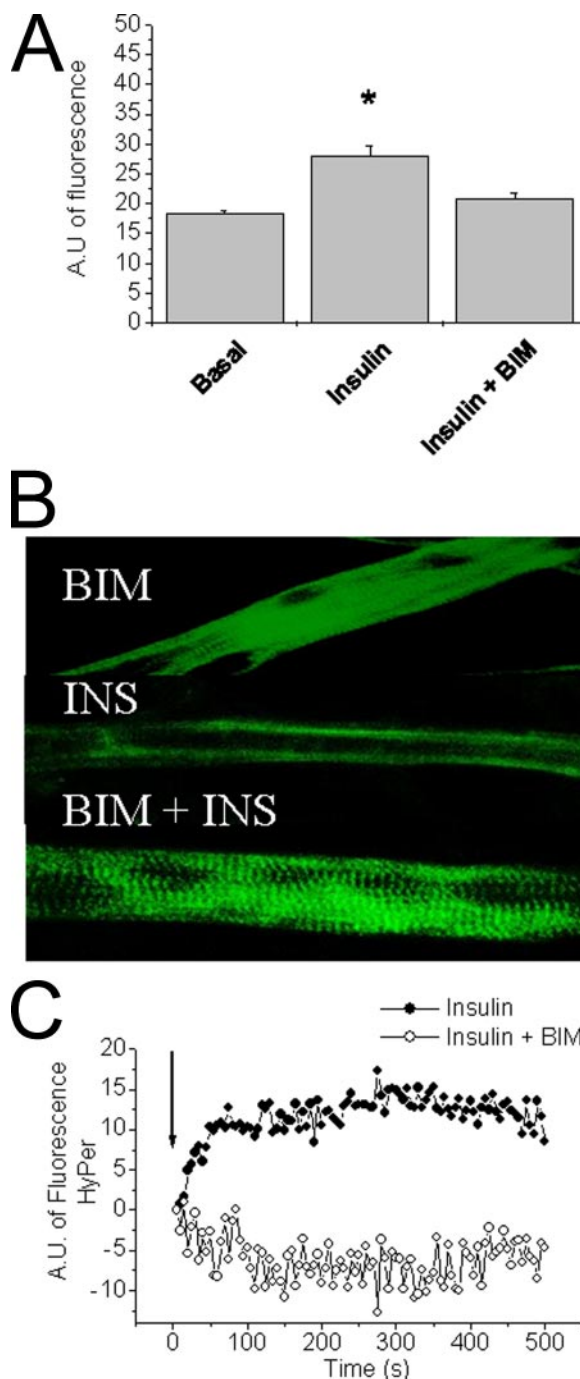


FIGURE 5. The role of PKC in H₂O₂ generation by insulin. A, mean fluorescence in myotubes loaded with CM-H₂DCFDA. Cells were preincubated with BIM (5 μM) for 30 min and were then stimulated with 50 nM insulin ($n = 8-13$, $p < 0.05$ (*)). A.U., arbitrary units. B, myotubes, control and incubated with 5 μM BIM, were stimulated with insulin (INS) and then fixed with methanol for 15 min to label with specific antibody against p47^{phox} (a representative image of three different cultures). C, time course of HyPer fluorescence of transfected myotubes in the presence or absence of BIM as indicated. The arrow shows insulin addition.

CM-H₂DCFDA as fluorescence probe and a molecular recombinant protein that *in vitro* displays half-maximal increase in fluorescence at 10 μM H₂O₂. CM-H₂DCFDA is a probe susceptible to oxidation by H₂O₂ and other ROS and nitric oxide-derived species, but transfection of myotubes with HyPer plasmid provided us with a specific tool to ascertain that 50 nM

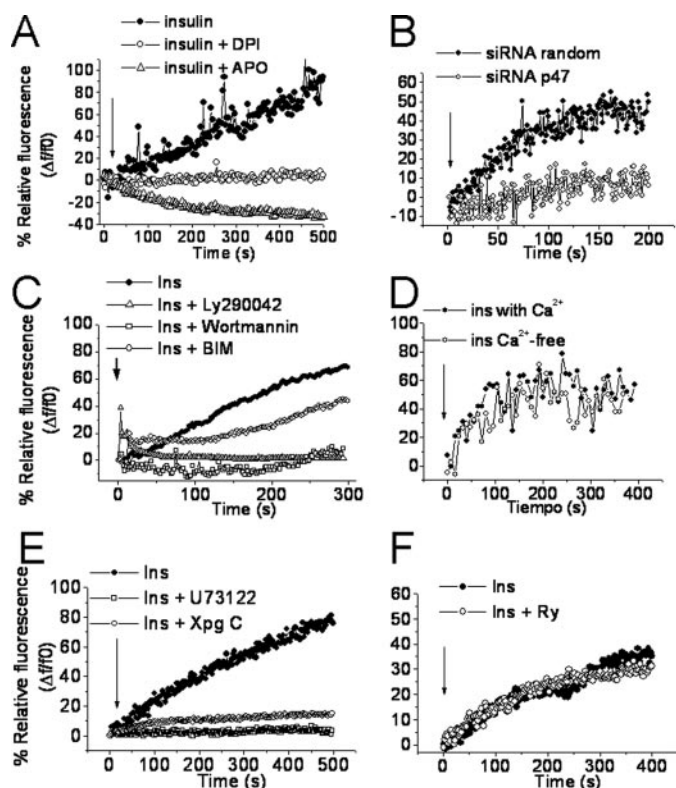


FIGURE 6. Ca^{2+} signals induced by insulin (*Ins*) in different conditions. The control curve of fluo-3 fluorescence was compared in each case with the same stimulus (50 nM insulin, *arrow*) in myotubes previously incubated or transfected in the following conditions. *A*, 50 μM diphenyliodonium (*DPI*) and 500 μM apocynin (*APO*). *B*, siRNA against p47^{phox} and an siRNA random. *C*, 50 μM LY290042, 100 nM wortmannin, and 5 μM BIM. *D*, Ca^{2+} -free condition (1 mM EGTA). *E*, 50 μM U73122 and 5 μM xestospingon C (*Xpg C*). *F*, overnight preincubation with 20 μM ryanodine (*Ry*, mean value of 6 experiments is shown).

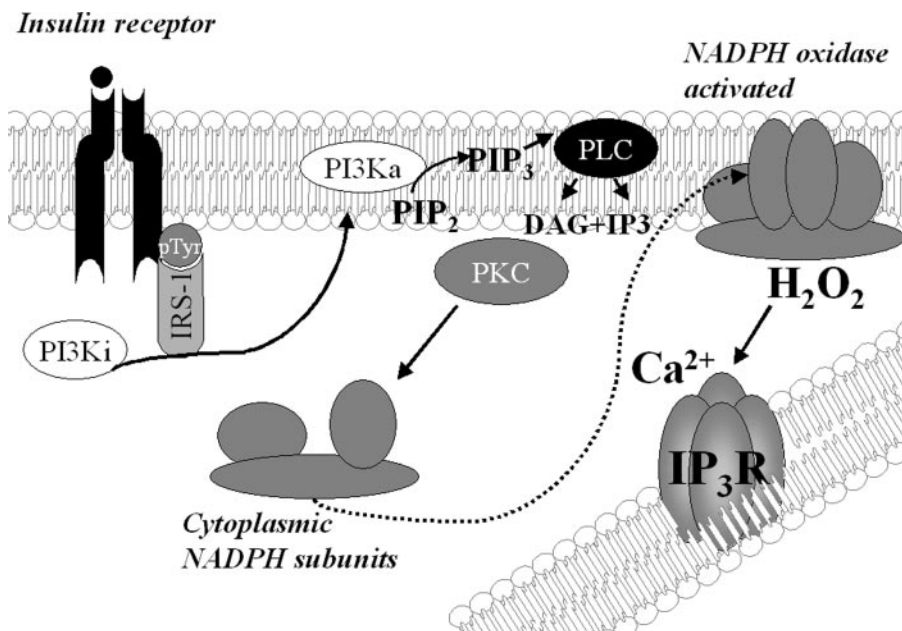


FIGURE 7. **Proposed mechanism for insulin-induced Ca^{2+} increase.** Insulin binds to its receptor in the plasma membrane, and binding promotes phosphorylation of its β subunit in tyrosine residues, recruiting IRS-1; binding of PI3K to IRS-1 activates inositol 1,4,5-trisphosphate (*PIP₃*) production, which stimulates phospholipase C γ (*PLC γ*) in the membrane to produce *IP₃* and DAG. DAG activates PKC δ , and this enzyme phosphorylates p47^{phox}, allowing this subunit to migrate to the membrane to form the activated NADPH oxidase complex; the resulting H_2O_2 modifies *IP₃* receptors and favors *IP₃*-induced Ca^{2+} release. *PIP₂*, phosphatidylinositol 4,5-bisphosphate; *pTyr*, phosphorylated tyrosine.

insulin produced H_2O_2 . An increase in intracellular peroxide concentration was detected with both probes as early as 1 min after insulin addition.

In various cell types, the NADPH oxidase has been described as the intracellular source of H_2O_2 (9). This enzyme has defensive functions in phagocytic cells, where it catalyzes the one-electron reduction of oxygen to release superoxide anion that rapidly dismutates to H_2O_2 , a microbicide agent. However, in non-phagocytic cells, H_2O_2 is considered a second messenger due to its capacity to produce reversible post-translational oxidative modification of proteins (18). We have reported previously that myotubes possess NADPH oxidase activity that is stimulated by membrane depolarization (1). Here, we provide evidence indicating that insulin also stimulates a p47^{phox}-dependent NADPH oxidase in skeletal muscle cells, as indicated by our findings that insulin-stimulated ROS generation was inhibited in myotubes preincubated with apocynin or transfected with an siRNA against p47^{phox}. In addition, our current results, showing p47^{phox} translocation from cytoplasmic striations to the plasma membrane from the first minute after stimulation with insulin (Fig. 3C), provide further support for NADPH oxidase activation by insulin.

Ca^{2+} signals mediate a variety of physiological processes in skeletal muscle cells; in particular, muscle depolarization elicits fast Ca^{2+} signals that initiate muscle contraction and slower signals that regulate gene expression (19). Insulin-dependent Ca^{2+} influx has been implicated in glucose uptake in adult muscle fibers (2); in that case, a delayed effect (after 20 min) of insulin that required external Ca^{2+} was reported. A direct link between NADPH-mediated ROS production and glucose uptake seems unlikely because a recent report showed no inhibition of glucose uptake by apocynin in insulin-stimulated skeletal muscle cell lines and primary cultures (20).

Insulin has been involved in the regulation of the expression of a number of skeletal muscle genes related to carbohydrate metabolism and protein synthesis (21). In skeletal muscle cells, Ca^{2+} release from *IP₃*-dependent intracellular stores mediates the regulation of signaling cascades, leading to expression or repression of both early and late genes (22–24). *IP₃* receptors are highly dependent on its regulators and modulators (25). A redox sensor protein has been shown to regulate type 1 *IP₃*R (26), redox-sensitive free thiol groups have been identified in the *IP₃*R molecule (27), and direct redox modifications of isolated *IP₃*R channels have been described (28). Accordingly, the Ca^{2+} signals elicited by insulin, which require NADPH oxidase and *IP₃* receptor activation, may also be

involved in regulation of gene expression. Further studies are needed to elucidate this point.

We have previously shown that electrical activity stimulates ROS production by NADPH oxidase in skeletal muscle cells and prompts the emergence of Ca^{2+} signals due to ROS-stimulated ryanodine receptors (1). Additionally, NADPH oxidase-generated ROS stimulate ryanodine receptor-mediated Ca^{2+} release from triad-enriched vesicles isolated from adult skeletal muscle cells (4). As electrical activity is a constant feature of functional muscle, insulin and electrical activity may jointly stimulate ROS generation, which by enhancing Ca^{2+} release mediated by ryanodine or IP_3 receptors, as shown in this work, generates Ca^{2+} signals that regulate muscle contraction or gene expression. In summary, we propose the following mechanism for insulin-dependent ROS production and delayed Ca^{2+} signal generation (Fig. 7). Insulin binding to its receptor promotes phosphorylation of its β subunit in tyrosine residues and recruits IRS-1; PI3K activation resulting from its binding to IRS-1 produces inositol 1,4,5-trisphosphate, which stimulates phospholipase C γ to produce IP_3 and DAG. The increased DAG production at the plasma membrane activates PKC δ , and this enzyme phosphorylates p47^{phox}, allowing this subunit to migrate to the membrane to form the activated NADPH oxidase complex; the resulting ROS modify IP_3 receptors and facilitate IP_3 -induced Ca^{2+} release, producing the delayed Ca^{2+} signals induced by insulin (Fig. 7).

Although insulin-enhanced Ca^{2+} release can certainly generate Ca^{2+} signals of physiological relevance on their own, insulin-derived H_2O_2 generation can also play an important role in muscle function. In fact, H_2O_2 as a messenger has been linked to the regulation of various redox-sensitive proteins, among them the ryanodine receptors (3, 29). Our results propose a new aspect of insulin-initiated signal transduction in skeletal muscle cells. We postulate an unexplored relationship between H_2O_2 production by insulin-stimulated NADPH oxidase and Ca^{2+} release mediated by IP_3 receptors, which may underlie insulin-dependent regulation of gene expression in muscle cells.

REFERENCES

1. Espinosa, A., Leiva, A., Pena, M., Muller, M., Debandi, A., Hidalgo, C., Carrasco, M. A., and Jaimovich, E. (2006) *J. Cell. Physiol.* **209**, 379–388
2. Lanner, J. T., Katz, A., Tavi, P., Sandstrom, M. E., Zhang, S. J., Wretman, C., James, S., Fauconnier, J., Lannergren, J., Bruton, J. D., and Westerblad, H. (2006) *Diabetes* **55**, 2077–2083
3. Hidalgo, C., and Donoso, P. (2008) *Antioxid. Redox Signal.* **10**, 1275–1312

4. Hidalgo, C., Sanchez, G., Barrientos, G., and Aracena-Parks, P. (2006) *J. Biol. Chem.* **281**, 26473–26482
5. Goldstein, B. J., Mahadev, K., Wu, X., Zhu, L., and Motoshima, H. (2005) *Antioxid. Redox Signal.* **7**, 1021–1031
6. Kamata, H., and Hirata, H. (1999) *Cell. Signal.* **11**, 1–14
7. Clempus, R. E., and Griendling, K. K. (2006) *Cardiovasc. Res.* **71**, 216–225
8. Mahadev, K., Motoshima, H., Wu, X., Ruddy, J. M., Arnold, R. S., Cheng, G., Lambeth, J. D., and Goldstein, B. J. (2004) *Mol. Cell. Biol.* **24**, 1844–1854
9. Bedard, K., and Krause, K. H. (2007) *Physiol. Rev.* **87**, 245–313
10. Bey, E. A., Xu, B., Bhattacharjee, A., Oldfield, C. M., Zhao, X., Li, Q., Subbulakshmi, V., Feldman, G. M., Wientjes, F. B., and Cathcart, M. K. (2004) *J. Immunol.* **173**, 5730–5738
11. Talior, I., Tennenbaum, T., Kuroki, T., and Eldar-Finkelman, H. (2005) *Am. J. Physiol.* **288**, E405–E411
12. Chowdhury, A. K., Watkins, T., Parinandi, N. L., Saatian, B., Kleinberg, M. E., Usatyuk, P. V., and Natarajan, V. (2005) *J. Biol. Chem.* **280**, 20700–20711
13. Frey, R. S., Gao, X., Javaid, K., Siddiqui, S. S., Rahman, A., and Malik, A. B. (2006) *J. Biol. Chem.* **281**, 16128–16138
14. Saltiel, A. R., and Kahn, C. R. (2001) *Nature* **414**, 799–806
15. Manders, E. M., Verbeek, F. J., and Aten, J. A. (1993) *J. Microsc. (Oxf)* **1993**, 375–382
16. Sanchez, G., Escobar, M., Pedrozo, Z., Macho, P., Domenech, R., Hartel, S., Hidalgo, C., and Donoso, P. (2008) *Cardiovasc. Res.* **77**, 380–386
17. Belousov, V. V., Fradkov, A. F., Lukyanov, K. A., Staroverov, D. B., Shakhbazov, K. S., Terskikh, A. V., and Lukyanov, S. (2006) *Nat. Meth.* **3**, 281–286
18. Rhee, S. G. (2006) *Science* **312**, 1882–1883
19. Jaimovich, E., and Espinosa, A. (2004) *Biol. Res.* **37**, 625–633
20. Hutchinson, D. S., Csikasz, R. I., Yamamoto, D. L., Shabalina, I. G., Wikstrom, P., Wilcke, M., and Bengtsson, T. (2007) *Cell. Signal.* **19**, 1610–1620
21. Rome, S., Clement, K., Rabasa-Lhoret, R., Loizon, E., Poitou, C., Barsh, G. S., Riou, J. P., Laville, M., and Vidal, H. (2003) *J. Biol. Chem.* **278**, 18063–18068
22. Powell, J. A., Carrasco, M. A., Adams, D. S., Drouet, B., Rios, J., Muller, M., Estrada, M., and Jaimovich, E. (2001) *J. Cell. Physiol.* **114**, 3673–3683
23. Carrasco, M. A., Riveros, N., Rios, J., Muller, M., Torres, F., Pineda, J., Lantadilla, S., and Jaimovich, E. (2003) *Am. J. Physiol.* **284**, C1438–C1447
24. Juretic, N., Urzua, U., Munroe, D. J., Jaimovich, E., and Riveros, N. (2007) *J. Cell. Physiol.* **210**, 819–830
25. Choe, C. U., and Ehrlich, B. E. (2006) *Science's STKE* **2006**, re15
26. Mikoshiba, K. (2007) *J. Neurochem.* **102**, 1426–1446
27. Joseph, S. K., Nakao, S. K., and Sukumvanich, S. (2006) *Biochem. J.* **393**, 575–582
28. Kaplin, A. I., Ferris, C. D., Voglmaier, S. M., and Snyder, S. H. (1994) *J. Biol. Chem.* **269**, 28972–28978
29. Feng, W., Liu, G., Allen, P. D., and Pessah, I. N. (2000) *J. Biol. Chem.* **275**, 35902–35907